EUV Hartmann sensor for wavefront measurements at the Free-electron LASer in Hamburg

Bernhard Flöter[1,3]**, Pavle Juranić**[2]**, Svea Kapitzki**[2]**, Barbara Keitel**[2]**, Klaus Mann**[1]**, Elke Plönjes**[2]**, Bernd Schäfer**[1] **and Kai Tiedtke**[2]

[1] Laser-Laboratorium Göttingen, Hans-Adolf-Krebs-Weg 1, D-37077 Göttingen, Germany
[2] Deutsches Elektronen-Synchrotron, Notkestraße 85, D-22603 Hamburg, Germany
E-mail: bernhard.floeter@llg-ev.de

Abstract. A compact, self-supporting Hartmann wavefront sensor was developed for the extreme ultraviolet (EUV) and soft x-ray range. The device is adapted to the characteristics of the Free-electron LASer in Hamburg (FLASH). It operates in a wavelength range from 6 to 30 nm with the capability to measure the wavefront quality of individual free-electron laser (FEL) pulses for beam characterization as well as for beamline alignment and monitoring behind user experiments. We report on online-Hartmann wavefront measurements at beamline BL2 with $\lambda_{13.5\,nm}/90$ accuracy for wavefront rms (w_{rms}). The results were used to align the ellipsoidal focusing mirror at the beamline, decreasing the residual root mean square (rms) wavefront aberrations by more than a factor of 3 to 2.6 nm. The spot size of 31 μm (x) and 27 μm (y) full-width at half-maximum (FWHM) as well as other beam parameters evaluated from wavefront and intensity data are consistent with independent profile measurements in the focal region, employing both a high-resolution EUV camera and poly(methyl metacrylate) (PMMA) imprints.

[3] Author to whom any correspondence should be addressed.

IOP Institute of Physics Φ DEUTSCHE PHYSIKALISCHE GESELLSCHAFT

Contents

1. Introduction

Free-electron lasers (FEL) generate coherent femtosecond x-ray pulses with unprecedented intensities. The peak brilliance of these novel x-ray sources exceeds that of modern synchrotron radiation sources by many orders of magnitude enabling new fields of science to be opened up for investigation, ranging from atomic, molecular and cluster physics to warm dense matter and surface dynamics, as well as diffraction imaging of small structures and biological samples ([1] and references therein). However, since currently operating x-ray FELs are based on the self-amplified spontaneous emission (SASE) process, which builds up the laser emission from electron shot noise, the photon beam characteristics relevant for the user experiments can differ from pulse to pulse. Therefore, there is a strong requirement for single-pulse photon diagnostics and online characterization of the beam propagation parameters [2, 3].

Hartmann–Shack and Hartmann wavefront sensors are already successfully applied for real-time laser beam characterization in the near infrared, visible and ultraviolet spectral region, recording simultaneously (i.e. in a single pulse) the wavefront (directional distribution) and the beam profile (intensity distribution) of a radiation field [4, 5]. A comprehensive and accurate evaluation of the relevant beam parameters such as beam width, divergence, M^2, Rayleigh length, waist position and waist diameter is possible from this information for coherent radiation, as has been shown in various articles [4, 6, 7]. Moreover, solving the Fresnel–Kirchhoff integral allows also numerical propagation of the beam, predicting the waist intensity distributions which are hard to measure for high-power laser radiation.

This paper reports on a compact extreme ultraviolet (EUV) wavefront sensor based on the Hartmann principle; it was jointly developed by Laser-Laboratorium Göttingen and DESY for photon diagnostics, beamline alignment and monitoring of FEL radiation at the Free-electron Laser in Hamburg (FLASH). Wavefront measurements were performed at the beamline BL2 at FLASH in the fundamental wavelength regime from 6 to 30 nm. The results of the Hartmann measurements at BL2 were compared to caustic measurements (cf section 2.2) to assess techniques for evaluation of focus size and position.
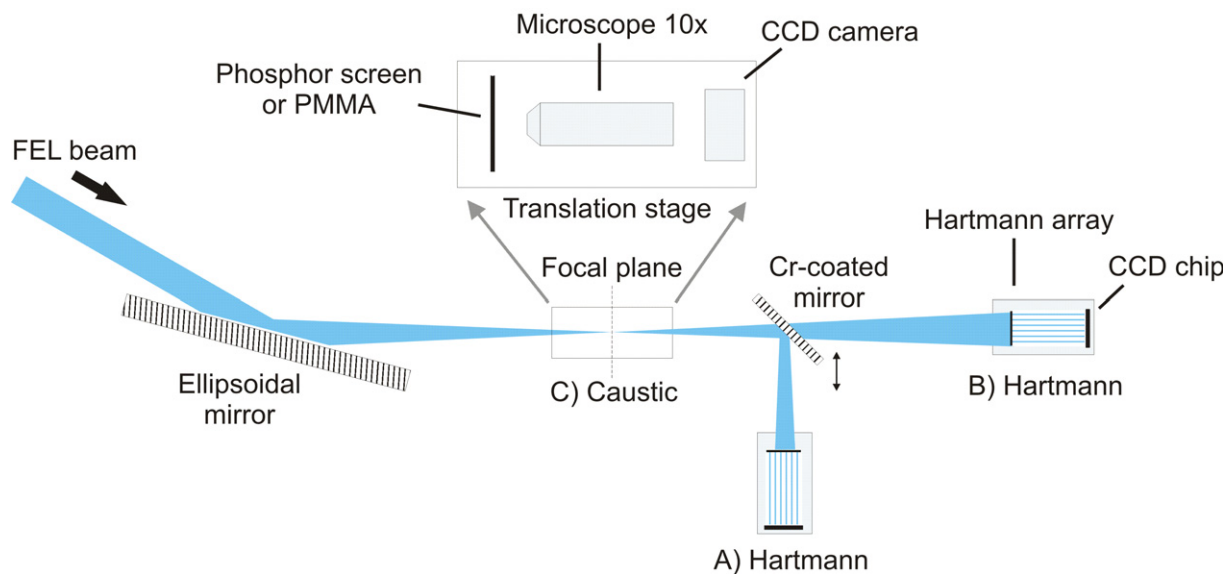
Figure 1. Experimental setup at BL2: the Hartmann sensor measures the wavefront either behind a plane chromium-coated mirror (A) or in the beam direction (B). The caustic sensor (a phosphorus screen imaged onto a charge-coupled device (CCD) chip by a $10\times$ magnifying microscope on a translation stage) examines the FEL beam at the focal plane of the ellipsoidal mirror (C).

2. Experiment and operation principle

Our experiments were conducted at the FLASH beamline BL2 using 13.8 and 25.9 nm wavelengths. The pulse structure of FLASH consists of 5 Hz bunch trains. Each train can be filled with 1–800 pulses at a repetition rate of 1 MHz. In addition, a fast shutter is integrated into the beamline system, which allows picking individual pulses.

At BL2, the beam is focused by a carbon-coated ellipsoidal mirror with 2 m focal length [2]. The extremely high brightness of FLASH poses a significant challenge for any type of profile measurements. Even in a single pulse the intensity has proven too high for the CCD chip used as detector, and different techniques of intensity attenuation were employed. As shown in figure 1, the Hartmann sensor was placed either in position A (about 3349 mm behind the ellipsoidal), where a Cr-coated mirror under $45°$ incidence angle was used as an attenuator, or in position B (about 4817 mm behind the ellipsoidal), making use of filters incorporated into the BL2 beamline and additionally into the wavefront sensor setup. The Cr mirror has a micro roughness of $\leqslant 1$ Å and a surface quality of $\lambda/30$–$\lambda/60$ (at 633 nm) over a 50 mm diameter, whereof only a section of 3 mm was illuminated. The sensor position is chosen such that the beam illuminates a sufficient number of subapertures. In addition, two caustic scans were performed through the focus (C, see figure 1), using a PMMA sample and a magnifying, phosphor-coated EUV camera. All experimental configurations with respect to positioning, filters, mirrors, apertures and wavelengths are summarized in table 1.

For the EUV camera measurements, the fundamental wavelength $\lambda = 25.9$ nm is efficiently blocked by the niobium filter (transmission 2.9×10^{-11}). Only the second and third harmonics at $\lambda = 13$ and 8.6 nm, which carry intensities of about 0.35 and 0.4% of the fundamental's

Table 1. Overview of the measurement positions, wavelengths and filters at BL2; positions relative to the ellipsoidal mirror (in the beam direction) are (a) 3349 mm, (b) 4817 mm, (c) ~ -50 m and (d) -3486 mm.

Measurement	Position	Filter	Mirror	Aperture	Fundamental wavelength
Hartmann	A[(a)]	–	Cr 45°	Ø3 mm[(c)]	25.9 nm
Hartmann	B[(b)]	Al 200 nm	–	Ø3 mm[(d)]	13.8 nm
EUV camera	C	Nb 202 nm	–	Ø3 mm[(d)]	25.9 nm
PMMA	C	–	–	Ø3 mm[(d)]	25.9 nm
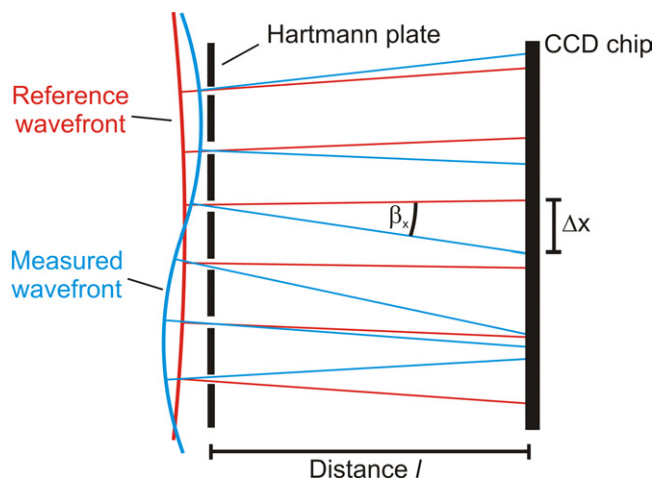
Figure 2. The incoming beam is divided into an array of beams by the Hartmann plate. The centroid deviation Δx from a known reference spot position divided by the distance l yields the local wavefront gradient β_x relative to the reference wavefront.

intensity prior to filtering [8], are transmitted. The pulse energy of ~ 30 nJ for both harmonics can be estimated from the average pulse energy of 20 μJ at 25.9 nm (measured with the FLASH gas monitor detector [9]) and the spectral filter transmission of the Nb filter [10]. For the Hartmann measurements at position A, the higher harmonics can be neglected owing to the reduced reflectivity of the Cr mirror. The Al filter used at position B attenuates the fundamental wavelength of 13.8 nm by a factor of 200.

2.1. The Hartmann sensor

The Hartmann sensor is based on a pinhole array that divides the incoming beam into an array of smaller beams, whose position and intensity are monitored with a CCD camera at a distance l from the array (see figure 2). The displacement of a spot centroid Δx divided by l yields the local wavefront gradient $\beta_{x,y}$ inside one subaperture relative to a known reference wavefront. In a modal approach using Zernike or Legendre polynomials, the wavefront $w(x,y)$ is reconstructed from the local gradients [11, 12] and afterwards corrected for tip/tilt and defocus [13]. A detailed

IOP Institute of Physics Φ DEUTSCHE PHYSIKALISCHE GESELLSCHAFT

description of the wavefront reconstruction methods is given in the references. Summation over pixel data inside the individual subapertures yields the intensity distribution or beam profile $I(x,y)$.

In the case of coherent radiation, the knowledge of the beam profile and wavefront allows calculation of the beam parameters using the moments method [4, 6, 14]. The central second spatial (x, y) and angular (u, v) moments are computed from the intensity distribution and the local wavefront slopes $\beta_{x,y}$ according to

$$\langle x^2 \rangle = \frac{\sum_{ij} \left(x_{ij} - \langle x \rangle \right)^2 I_{ij}}{\sum_{ij} I_{ij}}, \tag{1a}$$

$$\langle xu \rangle = \frac{\sum_{ij} \left(\beta_{x,ij} - \langle \beta_x \rangle \right) \left(x_{ij} - \langle x \rangle \right) I_{ij}}{\sum_{ij} I_{ij}}, \tag{1b}$$

$$\langle u^2 \rangle = \frac{\sum_{ij} \left(\beta_{x,ij} - \langle \beta_x \rangle \right)^2 I_{ij}}{\sum_{ij} I_{ij}} + \left(\frac{\lambda}{2\pi} \right)^2 \frac{\sum_{ij} \left((\partial_x I)^2 / I \right)}{\sum_{ij} I_{ij}}, \tag{1c}$$

where $\langle x \rangle$ and $\langle \beta_x \rangle$ are the first moments over x and β_x [6], and the index (ij) denotes the subaperture. This yields beam width d, divergence θ, beam propagation factor M^2, beam waist diameter d_0, Rayleigh length z_R and waist position z_0 according to the following equations [14]:

$$d = 4\sqrt{\langle x^2 \rangle}, \qquad \theta = 4\sqrt{\langle u^2 \rangle}, \tag{2a}$$

$$M^2 = \frac{4\pi}{\lambda} \sqrt{\langle x^2 \rangle \langle u^2 \rangle - \langle xu \rangle^2}, \tag{2b}$$

$$d_0 = \frac{4M^2\lambda}{\pi\theta}, \qquad z_R = \frac{d_0}{\theta}, \qquad z_0 = \frac{z_R \langle xu \rangle}{|\langle xu \rangle|} \sqrt{\left(\frac{d}{d_0} \right)^2 - 1}. \tag{2c}$$

Due to the high degree of spatial coherence reported for the FLASH beam [15], influences from partial coherence are neglected in this evaluation.

Once the intensity and the phase of the beam are known from the Hartmann measurement, the Fresnel–Kirchhoff propagation yields the intensity distribution at different propagation distances z,

$$I(x, y, z) = \left| \frac{ik}{2\pi z} \iint_\infty \sqrt{I(x', y')} e^{ikw(x'y')} e^{\frac{ik[(x-x')^2+(y-y')^2]}{2z}} \, dx' \, dy' \right|^2, \tag{3}$$

where x', y' and x, y are the Cartesian coordinates in two coplanar planes, separated by z.

The Hartmann wavefront sensor was designed to operate from 6 to 30 nm, which is within the accessible FLASH wavelength range. The Hartmann plate in the wavefront sensor consists of a 7 μm thick tantalum foil with circular laser-drilled holes in a square grid (pitch 320 μm, diameter 65 μm), distributed uniformly over a field of view of 8.25 mm × 6.6 mm. The spot patterns are recorded with a 12-bit digital CCD camera consisting of 1279 × 1023 pixels (size 6.45 μm). The CCD chip is mounted at a distance of 97 mm behind the Hartmann plate.
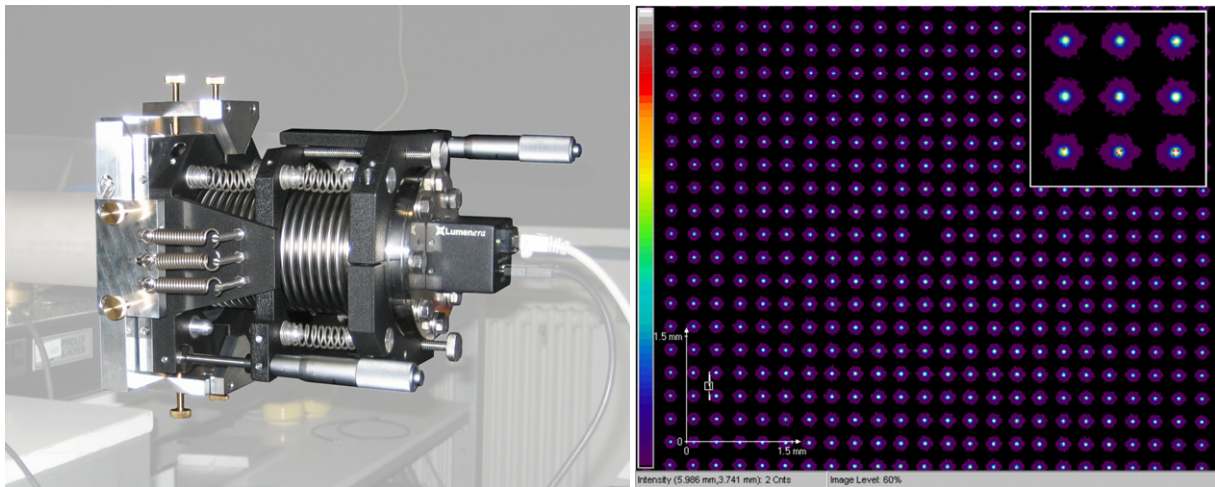
Figure 3. XUV Hartmann sensor with integrated tip/tilt and lateral adjustment (left) and spot pattern of the reference wavefront ($\lambda = 13.5$ nm, right). The central pinhole is omitted for tip/tilt alignment.

For EUV–visible conversion it is coated with a phosphorescent coating ($Gd_2O_2S:Tb$, grain size 1–2 μm, central emission wavelength 545 nm).

The Hartmann sensor (see figure 3) is adjustable both laterally and with respect to tip and tilt. The translational range is ± 10 mm and the tip/tilt range is $\pm 10°$, respectively. The device is self-supporting and compact (dimension 240 mm $\times$ 240 mm $\times$ 300 mm) and can be attached behind user experiments.

All wavefront measurements were performed with respect to a spherical reference wavefront, which was created by spatial filtering [5] at the FLASH beamline BL1 ($\lambda = 13.5$ nm). A 5 μm pinhole was placed 3870 mm in front of the Hartmann array, in the vicinity of the focal spot. The full field of view of the sensor was illuminated by half of the central Airy disc. The reference spot pattern consists of 10^3 averaged frames, each containing a single FEL pulse (cf figure 3, right).

Using the 5 μm pinhole and the same geometry as above, a series of single frames was recorded against this reference, yielding an average relative accuracy for a single frame, i.e. a wavefront repeatability of $\lambda/15$ w_{pv} (maximal wavefront peak-to-valley difference) or $\lambda/90$ w_{rms} (root-mean-squared) at $\lambda = 13.5$ nm. The values are obtained using a circular evaluation area of 19 subapertures in diameter. Tip/tilt and defocus are subtracted prior to the computation of w_{pv} and w_{rms} values.

The selection of the area of interest (AOI) for wavefront and beam profile evaluation is based on clipping of noise at a level of 1% of the full dynamic range of the camera. The largest circle inscribed into this AOI defines the evaluation radius.

2.2. Caustic measurements

Comparative caustic measurements were undertaken at BL2 ($\lambda = 25.9$ nm, cf table 1) along the beam waist behind the grazing incidence ellipsoidal mirror. Two methods were employed: imaging the FEL beam with a magnifying EUV camera and directly imprinting the beam on
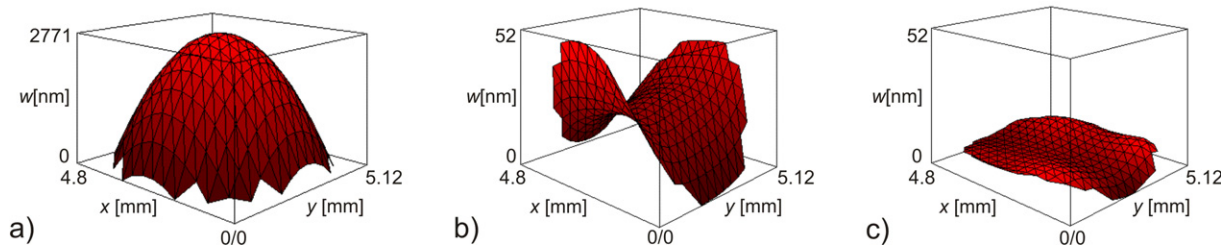
Figure 4. Initial wavefront at BL2 ($\lambda = 25.9$ nm) before mirror alignment including defocus term (a) and after subtraction of defocus (b), indicating strong astigmatism. After mirror alignment, w_{rms} was reduced from 9.2 to 2.6 nm and w_{pv} from 52 to 12 nm (c).

a PMMA sample [16]. A 3 mm circular aperture, which is installed in the FLASH beamline 3486 mm in front of the mirror, defined the beam area for all caustic measurements.

For the camera measurements at position C, the FLASH beam is attenuated by the niobium filter and converted to visible wavelengths by a phosphorescent coating (Gd_2O_2S:Tb) on a quartz substrate. This phosphor screen is installed on a vacuum window flange and imaged onto a CCD camera with a $10\times$ magnifying microscope objective outside the vacuum. The entire setup is mounted on a translation stage which moves along the optical axis (z) within $\sim 2z_R$ of each side of the focus (see figure 1 (C)). The peak fluence imposed on the phosphor at the focal spot was ~ 4 mJ cm^{-2}.

The phosphor screen was later replaced by a bulk PMMA sample (Goodfellow) to obtain single-shot imprints of the FEL beam at various z positions. From intensity measurements using the gas-monitor detector and the spot size determined later, we estimate a maximum fluence of ~ 500 mJ cm^{-2} in these experiments. The pulse energy was constant (except for beam fluctuations) for all z positions of each caustic scan. Depth profiles of the ablation craters (cf section 3.3) were obtained by white-light interferometry, yielding almost identical data as atomic force microscopy (AFM) scans. The intensity profile was reconstructed from the depth information, using Lambert–Beer's law including a threshold fluence for ablation. This approach is described in detail in [16, 17].

3. Results and discussion

3.1. Mirror alignment

A main objective for developing the EUV Hartmann sensor was the opportunity for optimizing the mirror alignment of the FLASH beamlines by online diagnostics. This is demonstrated for the grazing incidence ellipsoidal mirror at BL2 at a wavelength of 25.9 nm. For this purpose, the Hartmann sensor was placed behind the Cr-coated attenuating mirror (position A, see figure 1). A circular aperture (diameter 3 mm, 50 m in front of the focusing mirror) was used to adapt the beam size to the field of view of the sensor. In order to obtain a sufficiently high signal level and to improve the statistics, 30 bunches, each of $10\,\mu$J, were used for mirror alignment, averaged over ten camera frames. Before alignment, the tilt- and defocus-corrected wavefront showed a peak-to-valley (w_{pv}) of 52 nm and a root-mean-squared (w_{rms}) value of 9.2 nm (see figure 4) on a circular array of subapertures with 4.8 mm diameter. The dominating aberration
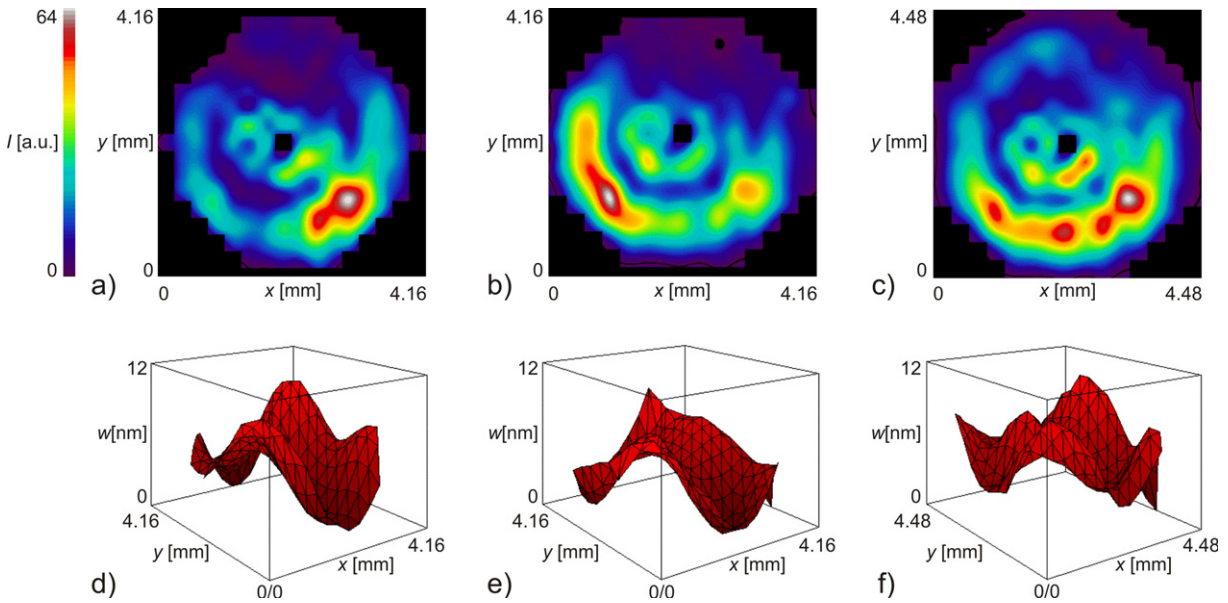
Figure 5. Intensity profiles (a–c) and corresponding wavefronts (d–f, after tip/tilt and defocus subtraction) of three single pulses at BL2 (Hartmann detector position A, $\lambda = 25.9$ nm, 3 mm aperture). The average w_{pv} value at this sensor position is 13.8 nm and the average w_{rms} is 2 nm.

was astigmatism oriented along the Cartesian coordinates, which could be reduced by real-time optimizing the pitch and yaw angles of the ellipsoidal mirror and by adjusting the remaining translational degrees of freedom. After alignment we found a w_{pv} of 12 nm and a w_{rms} of 2.6 nm ($\sim\lambda/10$). Relative to the pre-aligned initial position, the mirror was moved by -0.29 mrad (pitch) and -0.06 mrad (yaw).

3.2. Free-electron laser (FEL) beam characterization from Hartmann data

After optimization of the ellipsoidal mirror adjustment, Hartmann measurements from single bunches of FLASH were performed at BL2 (detector position A, cf figure 1), using a circular aperture in the beamline (diameter 3 mm, placed 50 m in front of the focusing mirror). Intensity distributions and corresponding wavefronts for a FLASH wavelength of $\lambda = 25.9$ nm are displayed in figure 5. The wavefronts were reconstructed from a circular array of spots (diameter 4.16 or 4.48 mm, depending on beam width fluctuations); related beam profiles are obtained by integration over pixel counts in individual subapertures, followed by an adapted spline interpolation.

All beam profiles show a distinct annular diffraction pattern, caused by the circular aperture, with superimposed pulse-to-pulse fluctuations. In addition to the International Organization for Standardization (ISO) beam parameters (2a)–(2c) evaluated from single-intensity distributions (e.g. beam width, uniformity), consecutive profile acquisition also provides information on the positional stability and the amount of profile fluctuations. For the profiles displayed in figures 5(a)–(c), the beam positional stability is evaluated from the standard deviation of the centroids (first moments), yielding a value of about $\pm 350\,\mu$m ($\pm\sigma$) for x and y.

Table 2. Wavefront and beam parameters obtained for sensor position B ($\lambda = 13.8$ nm, 3 mm aperture and 200 nm Al filter).

w_{pv}	10.6 nm(± 1.6 nm)
w_{rms}	1.6 nm(± 0.2 nm)
Waist position z_{0x} (horizontal)	2060 mm after the focusing mirror
Waist position z_{0y} (vertical)	2068 mm after the focusing mirror
Waist diameter (2nd moment) d_{0x} (horizontal)	53 μm($\pm 5\,\mu$m), relates to 31 μm FWHM
Waist diameter (2nd moment) d_{0y} (vertical)	45 μm($\pm 4\,\mu$m), relates to 27 μm FWHM
Beam propagation factor M^2	4.1(± 0.3)

FWHM, full-width at half-maximum.

The single bunch wavefronts depicted in figure 5 (below) indicate a w_{pv} deformation around 13.8 nm ($\sim\lambda/2$) after tip/tilt and defocus subtraction, corresponding to a w_{rms} value of 2 nm ($\sim\lambda/16$). The overall pulse-to-pulse wavefront fluctuations in terms of w_{pv} and w_{rms} are of the order of 10–20% of the average values.

Similar Hartmann measurements were also performed at position B of BL2 ($\lambda = 13.8$ nm, with 3 mm aperture and 200 nm Al filter) in the direct FEL beam, yielding almost identical w_{pv} and w_{rms} values. From these measurements the single bunch beam parameters shown in table 2 were evaluated according to (2a)–(2c), using a circular evaluation area with 14 subapertures diameter.

For ease of comparison of the waist diameters, FWHM values are also indicated, presuming a Gaussian beam profile with the same second moment diameter as the measured pulse. The numerical aperture for these measurements was approximately 7.5×10^{-4}, which follows from the 3 mm aperture and the focal length of the ellipsoidal mirror. The diffraction limited focal spot diameter for $\lambda = 13.8$ nm is 9 μm (FWHM of Airy pattern).

3.3. Comparison with caustic measurements

The beam parameters listed above were compared to data obtained from caustic measurements at position C ($\lambda = 25.9$ nm). Corresponding EUV camera beam profiles and ablative imprints in PMMA are displayed in figure 6, together with a numerical propagation of the Hartmann data (intensity and phase distribution) through the focal region, using the Fresnel–Kirchhoff integral (3). All measured caustic profiles and computational results agree both in shape and size.

Figure 6(a) shows the numerical back propagation from sensor position B based on a circular AOI with 4.48 mm diameter, and figure 6(b) shows the propagation from position A backwards using 5.12 mm evaluation diameter. Both propagations yield similar intensity distributions with respect to beam width and shape. Compared to the intensity profiles obtained from the EUV camera shown in figure 6(c), the propagated distributions are a bit more structured. These artificial spots can be attributed to the limited intensity sampling of the Hartmann data. White-light interferometric micrographs of single-pulse PMMA imprints are displayed in figure 6(d) indicating sharp edges due to the ablation threshold of the material. Depth profiles of the ablation craters were converted into intensity distributions following Lambert–Beer's law with an interpolated ablation threshold of 7.2 mJ cm^{-2} according to [16] and an absorption length of 55.2 nm [10].
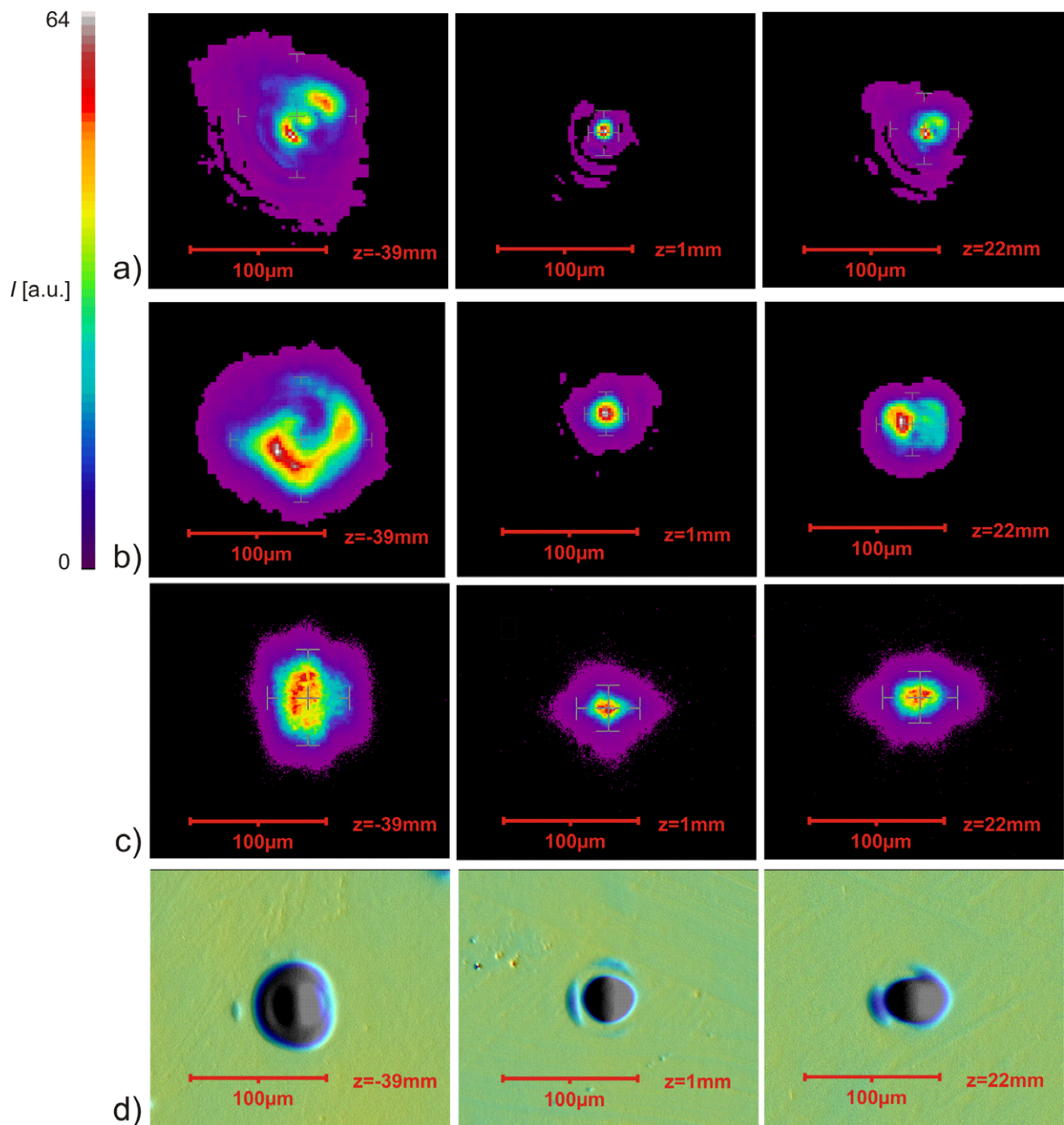
Figure 6. Calculated (a, b) and measured (c, d) caustic scans through the focal region of the FLASH beam at BL2. The pictures show numerical propagation using the Fresnel–Kirchhoff integral from Hartmann sensor position B backwards (row a), and from position A backwards (row b), single-pulse EUV camera beam profiles (row c) and ablative PMMA imprints (white-light interferometry, row d). The z position is given with respect to the waist location for each row. The intensity is given in arbitrary units scaled to the maximum intensity for each plot.

Table 3. Summary of the beam parameters determined from Hartmann measurement, caustic measurement with EUV camera and caustic measurement using PMMA imprints. The EUV camera M^2 value is given with respect to a wavelength of 10.8 nm, which accounts for the spectral transmissivity of the niobium filter. For comparison, the FWHM waist diameters are indicated presuming a Gaussian beam.

	Hartmann		EUV camera		PMMA	
	x	y	x	y	x	y
z_R (mm)	34	30	29	22	28	24
z_0 (mm)	2060	2068	1985	1996	1991	2000
d_0 (mm) 2nd moment	53	45	42	32	31	27
d_0 (mm) FWHM	31	27	25	19	18	16
θ (mrad)	1.56	1.53	1.47	1.47	1.11	1.13
M^2	4.7	3.9	4.6	3.4	–	–

For a quantitative comparison with the propagated Hartmann data, second moment beam diameters were computed from single-pulse intensity profiles, averaging the beam diameters of 6 profiles (PMMA) and 100 profiles (EUV camera). A quadratic fit of the averaged second spatial moments as a function of z around the beam waist was performed (PMMA: 9 different z positions; EUV camera: 32 different z positions). From the fit parameters the beam propagation factor M^2, the waist diameter d_0 and the waist position z_0 are obtained [14]. It should be noted, however, that in contrast to the Hartmann measurement, the caustic evaluation yields only averaged beam parameters and does not offer single pulse resolution.

All relevant beam parameters obtained from the three different characterization methods are compiled in table 3. The M^2 value is 3.9 for the EUV camera (computed as square root of $M_x^2 \cdot M_y^2$ in simple astigmatic approximation) and 4.1 for the Hartmann sensor, indicating good agreement between these two methods with only 5% deviation. This holds also for the divergence data that differ by less than 6%, as well as for the waist positions deviating by 3%. The latter corresponds to an uncertainty of approximately 25 mm in the radius of curvature of the Hartmann reference wavefront, which is within the accuracy of the experimental setup.

We used Zernike polynomials representing aberrations up to fifth order (15 coefficients excluding piston). This includes the vital third order, which is representing well the typical misalignment effects (see figure 4) and avoids higher order terms which are more affected by noise. The waist position does not depend critically on the polynomial degree since the wavefront is mainly dominated by the defocus term, and the sensor position is many Rayleigh lengths away from the focal spot.

Lateral stability of the focal spot was determined by computing the first spatial moments of single-pulse EUV camera intensity profiles, yielding a focal spot displacement of $\pm 2\,\mu$m ($\pm\sigma$). Axial focal spot stability follows from consecutive single-pulse Hartmann measurements (section 3.2). The stability along the optical axis is below ± 1.5 mm (standard deviation of focal spot positions with the sensor on position A).

The waist diameters d_0 are two to three times larger than the diffraction-limited spot size of 9 μm (FWHM), which can be explained by the relatively large beam propagation factor. The

deviations of the evaluated waist diameter data can clearly be attributed to specific experimental problems of the different techniques:

- *Hartmann sensor*: The limited spatial sampling imposes errors on the propagated profiles. Thus, a wavefront sensor with higher resolution (smaller pitch of Hartmann array) is currently under development.

- *Caustic measurement using an EUV camera*: The quantum converter employed shows a weak nonlinear response (peak fluence $\sim 4\,\mathrm{mJ\,cm^{-2}}$). Such saturation effects may not be accounted for properly. Nonlinearity tends to result in accurate waist position determination but overestimated waist size, Rayleigh lengths and beam propagation parameters.

- *Caustic measurement using PMMA*: The PMMA imprints yield the smallest spot diameter of all three characterization techniques. The measured results depend critically on the ablation threshold of PMMA, which leads to a truncation of the beam profile. The beam propagation factor obtained from the PMMA imprints in our experiment is underestimated and non-physical. This hints at underestimated beam diameters for z positions further away from the waist.

In addition, the beam width of single FLASH pulses fluctuates by $\sim 10\%$ (2σ) around the mean beam diameter. The imposed error is relevant mainly for the PMMA profiles, where significantly fewer pulses were averaged. Another complication results from the influence of higher harmonics, since the FLASH fundamental wavelength and the filters differed between the measurements. The beam parameters for the EUV camera were computed with respect to a mean wavelength of 10.8 nm calculated from the spectral transmissivity of the filter and the spectral content of the FLASH beam.

4. Conclusion

The presented measurements prove the feasibility of a compact EUV Hartmann wavefront sensor to be employed under FEL conditions in the EUV spectral region. The self-supporting device allows simultaneous recording of both wavefront and intensity distributions of single FEL pulses, accomplishing an analysis of beam fluctuations. By averaging over several pulses, the sensor could be utilized to align the ellipsoidal focusing optics of beamline BL2 at FLASH, yielding a reduction of the residual wavefront aberrations (w_{rms}) from 9.2 nm ($\lambda/3$) to 2.6 nm ($\lambda/10$) at $\lambda = 25.9$ nm.

From wavefront and intensity profile data the characteristic propagational parameters of the FEL beam were computed, in particular divergence, waist position and waist diameter. These results were compared to data obtained from standard beam characterization techniques. At this, a quantum converter-based EUV microscope camera as well as PMMA imprints were employed to record intensity profiles in the near-focal region. General agreement between these two different sets of caustic measurements and the Hartmann approach is found. Still existing deviations can be explained by specific shortcomings of each technique, i.e. the significant ablation threshold of PMMA and the nonlinearity of the phosphor screen used in the EUV camera.

As opposed to the caustic measurements, the Hartmann sensor provides wavefronts and intensity profiles of single FEL pulses and can easily be placed behind a user experiment for online diagnostics. For a further improved prediction of the propagation characteristics,

IOP Institute of Physics ⬥ DEUTSCHE PHYSIKALISCHE GESELLSCHAFT

a wavefront sensor with a higher dynamic range and higher spatial resolution (smaller array pitch) is currently being developed.

Acknowledgments

References

[1] Bostedt C *et al* 2009 Experiments at FLASH *Nucl. Instrum. Methods* A **601** 108–122
[2] Tiedtke K *et al* 2009 The soft x-ray free electron laser FLASH at DESY: beamlines, diagnostics and end-stations *New J. Phys.* **11** 023029
[3] Kuhlmann M *et al* 2006 Wave-front observations at FLASH *Proc. FEL 2006* (Berlin: BESSY) p 794
[4] Schäfer B, Lübbecke M and Mann K 2006 Hartmann–Shack wave front measurements for real time determination of laser beam propagation parameters *Rev. Sci. Instrum.* **77** 053103
[5] Mercère P *et al* 2003 Hartmann wave-front measurement at 13.4 nm with accuracy *Opt. Lett* **28** 1534–6
[6] Schäfer B and Mann K 2002 Determination of beam parameters and coherence properties of laser radiation by use of an extended Hartmann–Shack wave-front sensor *Appl. Opt* **41** 2809–17
[7] Neal D R, Alford W J, Gruetzner J K and Warren M E 1996 Amplitude and phase beam characterization using a two-dimensional wavefront sensor *Proc. SPIE* **2870** 72–82
[8] Düsterer S *et al* 2006 Spectroscopic characterization of vacuum ultraviolet free electron laser pulses *Opt. Lett.* **31** 1750–2
[9] Tiedtke K *et al* 2008 Gas detectors for x-ray lasers *J. Appl. Phys.* **103** 094511
[10] Henke B L, Gullikson E M and Davis J C 1993 X-ray interactions: photoabsorption, scattering, transmission, and reflection at $E = 50$–30000 eV, $Z = 1$–92 *At. Data Nuclear Data Tables* **54** 181–342
[11] Cubalchini R 1979 Modal wavefront estimation from phase derivative measurement *J. Opt. Soc. Am.* **69** 972–977
[12] Noll R J 1978 Phase estimates from slope type wavefront sensors *J. Opt. Soc. Am.* **68** 139–40
[13] ISO 15367-2 2005 Lasers and laser-related equipment—test methods for determination of the shape of a laser beam wavefront
[14] ISO 11146-1 2005 Lasers and laser-related equipment—test methods for laser beam width, divergence angle and beam propagation ratio
[15] Singer A, Vartanyants I A, Kuhlmann M, Duesterer S, Treusch R and Feldhaus J 2008 Transverse coherence properties of the free-electron laser FLASH at DESY *Phys. Res. Lett.* **101** 254801
[16] Chalupsky J *et al* 2007 Characteristics of focused soft x-ray free-electron laser beam determined by ablation of organic molecular solids *Opt. Express* **15** 6036–43
[17] Chalupsky J *et al* 2009 Non-thermal desorption/ablation of molecular solids induced by ultra-short soft x-ray pulses *Opt. Express* **17** 208–17